POTENTIAL OF POWER RECOVERY OF AN AXIAL FAN IN WINDMILLING OPERATION

S. COURTY-AUDREN [1,2] - N. BINDER [1] - X. CARBONNEAU [1] - F. CHALLAS [2]

(1) Université de Toulouse, ISAE
10, avenue Edouard BELIN BP 54032
31055 Toulouse Cedex 4
France
suk-kee.courty-audren@isae.fr - nicolas.binder@isae.fr - xavier.carbonneau@isae.fr

(2) SAFRAN - Technofan
10, place Marcel DASSAULT BP 30053
ZAC du Grand Noble
31702 Blagnac cedex
France
florent.challas@technofan.com

ABSTRACT

During the last decades, efforts to find efficient green energy solutions have been widely increased in response to environmental concerns. Among all renewable energies, this paper is focused on wind power generation. To this end, a windmilling axial fan in turbine operation is experimentally and numerically investigated. Under specific conditions, the studied fan is naturally freewheeling. Consequently, the main objective of this analysis is to determine whether or not this intrinsic windmilling behavior can be optimized for power generation. A preliminary study of the fan is dedicated to the knowledge of the fan characteristics in normal operating conditions. Then, two windmilling configurations (direct and reverse flow direction) are tested and compared on the basis of the output power. An analysis of the velocity triangle gives the opportunity to evaluate the energy recovery potential of both solutions. Of the two, the reversed configuration showed a higher level of output power than the direct one.

NOMENCLATURE

ΔH	Enthalpy variation	W	Power [kW]
N	Rotational speed [RPM]	α	Absolute flow angle [deg]
Q	Mass flow rate [$kg.s^{-1}$]	β	Relative flow angle [deg]
r	Radius [m]	η	Efficiency
S	Section [m^2]	π	Pressure ratio
U	Blade speed [m/s]	ρ	Density [$kg.m^{-3}$]
V	Flow absolute velocity [m/s]	ϕ	Flow coefficient
W	Flow relative velocity [m/s]	ψ	Loading coefficient

SUBSCRIPT & SUPERSCRIPT

θ	Tangential direction	1	Rotor inlet
x	Axial direction	2	Rotor outlet
T	Total quantity	$.^*$	Reduced quantity, in % of the design point value
r	Relative frame		
Hub	Referring to hub (surface, radius)	c	Compressor (pressure ratio)
Tip	Referring to casing (surface, radius)	Shaft	Available on shaft (power)

I. Introduction

In the open literature, publications related to windmilling generally aim at estimating freewheeling engines drags [1] and relighting capabilities [2]. The term freewheeling describes an unbraked spontaneous rotation of turbomachine stages caused by an incoming airflow. The cases of study are mostly multistage turbomachinery with large diameter meant for propulsion applications [3]. Both the finality and the stage architecture of the present work are thus unusual for a windmilling situation. Indeed, the considered fan, composed of one mono-stage rotor/diffuser, is investigated in a view to determining its potential of power generation. The amount of energy recovered by this fan when operated in windmilling needs to be quantified.

Few equivalent configurations are found in the literature. In 2010, Prasad [4] showed that in freewheeling mode, a turbofan rotor runs both as turbine and as compressor in the span-wise direction. Based on total temperature variations and angle deviation, the author identifies turbine-like and compressor-like regions, the inner blade sections acting like compressor and the upper sections like turbine. The two effects are nearly cancelling each other so that the resulting work, related to the angle deviation through the Euler theorem, is approximately zero. This lack of deviation comes as an explanation of the vane blockage (massive flow separation) since the stator operates at highly negative incidence. The author also shows numerical results, obtained with the NUMECA FINE^{TM}/Turbo suite software, in order to analyze flow structures such as flow separation and vane blockage. Anyway, the lack of resistive torque applied on the shaft probably also explains the fact that the turbine naturally finds a configuration in which very little energy is recovered.
On the contrary, Gill (2012) [5] recently studied an axial compressor in reversed windmilling configuration through a numerical approach carried out with the same FINE^{TM}/Turbo software. The results show little flow separations both on rotor and stator blades. In this configuration, the maximum turbine efficiency reaches values around 76%. The author explains this unexpected good performance by the lack of separation and the thin-shaped wakes observed in numerical results.

In this study, both of these approaches, namely a direct-flow turbine mode (*Direct Mode*) and a reverse-flow turbine mode (*Reverse Mode*), are tested on a mid-sized fan by experimental and numerical methodologies. The aim of this study is to characterize the potential of power generation of this fan which considered as a possible additional onboard power source for aircrafts applications. First, a theoretical background is recalled, in the insight of energy recovery. Then, the methodologies are presented. Fan and windmilling results are exposed in two following sections. Finally, a conclusion gives the opportunity to discuss the results.

II. Theoretical background

In this section, the energy recovery potential of a mid-sized fan is evaluated through a local analysis of the flow configuration. On this fan at maximum rotational speed, the characteristic Mach number at the tip of the blade is M ≈ 0.29. The fan is thus at the frontier of the validity of the hypothesis of incompressible flows. In that situation, as reported by Lakshminarayana [6], some usual parameters used in the description of the operating point of a turbomachine are no more relevant. Both the influences of the Mach number and of the rotational speed can be neglected. The Reynolds number variations are supposed small, compared with its typical value. It means that a more convenient representation of the stage operation than the usual map exists. It can be found in map involving the flow coefficient, ϕ, and the loading coefficient, ψ, defined as follow:

$$\phi = \frac{V_{1,x}}{U} \tag{1}$$

$$\psi = \frac{\Delta H}{U^2} \tag{2}$$

The axial velocity at the rotor inlet, $V_{1,x}$, is (supposed) uniform so that it can be evaluated anywhere in this section. In this development, it is estimated for a given constant radius defined in Eq.(3). It is experimentally derived from the mass flow rate divided by the density and the inlet rotor surface. A

simple relation between these coefficients and the geometry of the stage can be derived. To this end, conventional velocity triangles are presented for the two studied windmilling configurations (Figure 1), in order to illustrate the theoretical development.

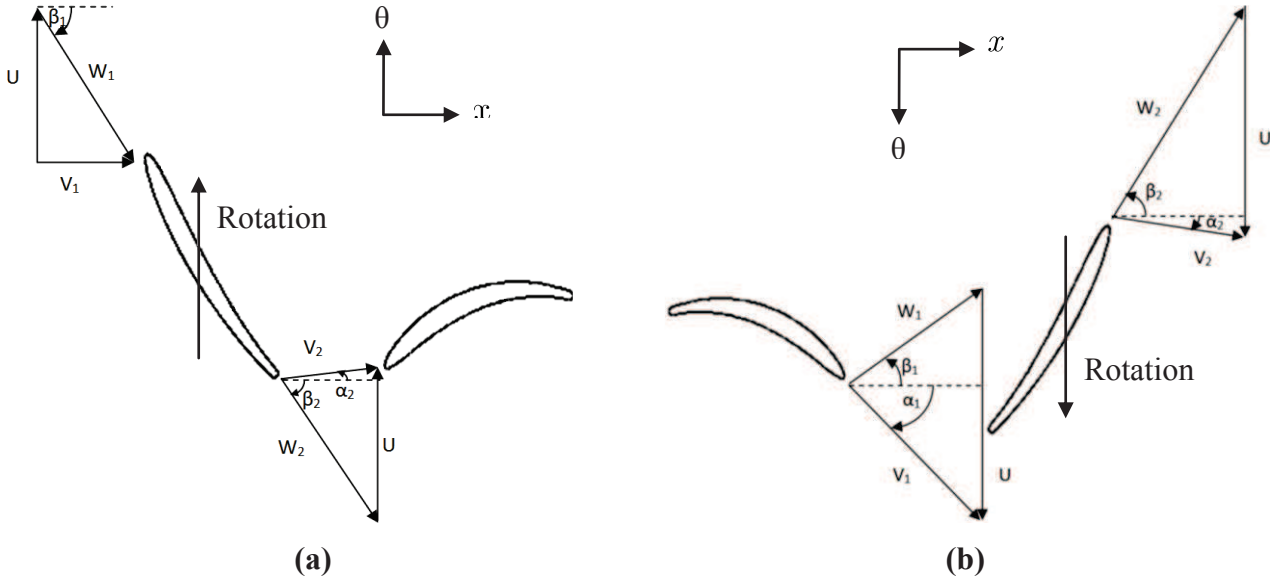

Figure 1. Velocity triangles, (a) *Direct Mode* - (b) *Reverse Mode*

For axial machines, the blade velocity U, appearing in eq. (1) and eq. (2), is not constant along the radial direction. In this paper, all the relations are expressed at the mean section radius defined in eq.(3)

$$r = \sqrt{\frac{S_{tip} - S_{hub}}{\pi}} = \sqrt{\frac{\pi r_{tip}^2 - \pi r_{hub}^2}{\pi}} \tag{3}$$

The loading coefficient, ψ, can be expressed as:

$$\psi = \frac{P_{shaft}}{QU^2} \tag{4}$$

In chapters IV and V, the loading coefficient is experimentally evaluated according to eq.(4) since power, masse flow and blade speed are recorded for every operating point tested. Furthermore, according to the Euler theorem, the expression of the loading coefficient eq.(2) can also be reduced to:

$$\psi = \frac{\Delta(UV_\theta)}{U^2} \tag{5}$$

For axial fan, the blade velocity, U, is considered constant along a blade at fixed span position due to constant radius and rotational speed. At this point, the usual assumption of a purely axial flow at the inlet plane of the rotor is made, for both *Fan Mode* and *Direct mode*. Consequently, the expression of the loading coefficient can be simplified in eq.(5), since, $V_{\theta 1} = 0$.

$$\psi = \frac{V_{\theta 2}}{U} \tag{6}$$

Usual relationship between tangential flow velocity, axial flow velocity and blade speed leads to eq.(8):

$$\psi = \frac{U - V_{x,2} \tan \beta_2}{U} \tag{7}$$

Since the flow is supposed incompressible, the axial velocity variation is neglected. Then:

$$\psi = 1 - \phi \tan \beta_2 \tag{8}$$

It means that all the operating points of both the *Fan Mode* and the direct-flow *Direct Mode* should collapse on a single trend in a ψ- ϕ map. This is also true for the *Reverse Mode* for which the presence of the diffuser upstream creates a pre-swirl. Eq. (8) thus becomes:

$$\psi = 1 - \phi(\tan\alpha_1 + \tan\beta_2) \quad (9)$$

From the expressions of Eq. (8) and (9), some comments can be made in the insight of energy recovery.

- First, both the operating points of the *Fan Mode*, and that of the *Direct Mode* should collapse on the same trend in the ψ-ϕ map. Obviously, the positive region for ψ represents the *Fan Mode*, and the negative region represents the *Direct Mode*. The intercept point of the x-axis (ψ =0) is only a function of the stage outlet angle, assuming that flow deviations are negligible.

- Second, due to this continuity, it will never be possible to recover the same amount of energy in the direct-flow turbine mode (*Direct Mode*) for a given flow across the stage as the one expensed in the *Fan Mode*.

- Finally, it appears clearly from both Figure 1 and Eq. (9) that the flow absolute deviation at the inlet of the stage increases the power recoverable for the *Reverse Mode*.

To check the validity of these three assessments, both numerical and experimental methodologies are set up.

III. Methodology

III.1. Studied fan characteristics

In this section, the studied fan is presented. As mentioned in the introduction, it is an electrical subsonic axial fan. The stage is composed of a rotor wheel and of a vaned diffuser. For confidentiality reasons, only orders of magnitude are given to describe its geometrical characteristics.

Casing radius	Lower than 200 mm	Nominal Power consumption	Around 2 kW
Hub radius	Higher than 100 mm	Nominal mass flow	Around 1 kg/s
Axial size	Around 250 mm	Number of stator blades	23
Nominal rotational speed	Around 10 000 RPM	Number of rotor blades	17

Table 1. Geometrical characteristics of the investigated fan

III.2. Experimental devices

In this section, fan and windmilling test benches are described. The fan is integrated in an instrumented carter, which can be plugged in different test benches. Three resulting configurations have been tested and are illustrated in Figure 2 (a) & (b).

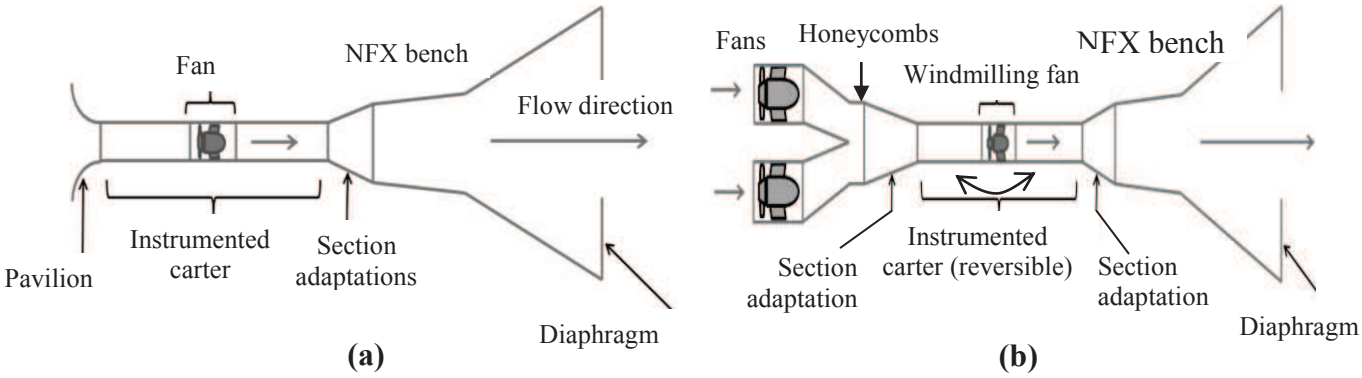

Figure 2. (a) Fan test bench - (b) Windmilling test benches (*Direct & Reversed*)

In the *Fan Mode* (Figure 2 (a)), an electrical engine drives the rotor. This engine is powered by 200V/400Hz three-phase sources. The flow is ingested through a nozzle duct, called pavilion on Figure 2 (a). The windmilling *Direct Mode* corresponds to typical windmilling configuration characterized by a usual airflow direction (Figure 2 (b)). The flow is forced by the use of two additional fans. This airflow rotates the rotor row, which is consequently in windmilling. The mechanical braking torque on the shaft is controlled by the electrical engine, which is now used as a generator, using variable loadings. Generator loadings are modified by the use of different configurations of outlet impedance. An atypical windmilling configuration, called *Reversed Mode*, obtained by turning the instrumented carter top-to-tail is also experimentally tested (Figure 2 (b)). In that case, air first goes through the fan diffuser and leaves the stage from the rotor row.

III.3. Instrumentation and Data acquisition

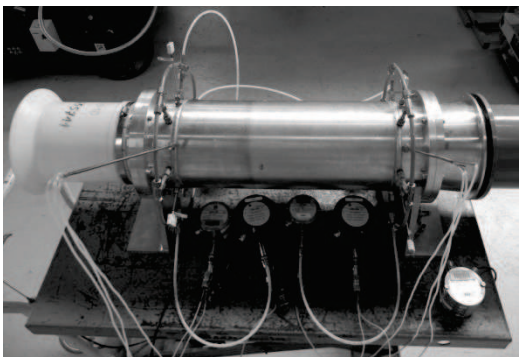

- S1 & S3: 6-hole Kent chambers
- S2 & S4: 3 total temperatures, 1 total pressure

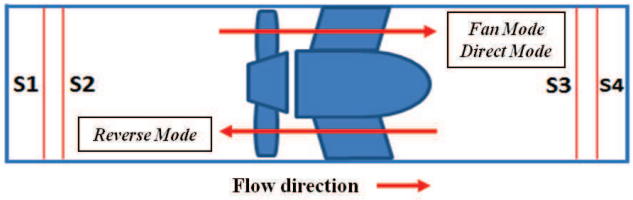

(a) (b)

Figure 3. (a) Picture of the instrumented carter - (b) Schematic of the measurement sections

The instrumented carter is composed of 6 total temperature sensors, 2 total pressure sensors, and 2 static pressure sensors. Atmospheric temperature and pressure are also recorded as well as NFX outlet static pressure and total temperature (Figure 3 (a) & (b)). The fan efficiency is calculated thanks to the ISO 5801 norm procedure [7] through classical inlet/outlet measurements. The volume flow rate and the total pressure rise are also obtained with the ISO 5801 norm. Calculations of these quantities are based on atmospheric conditions, static pressure and total temperature measurements at the NFX bench outlet. Static measurements are also performed from tappings in sections 1 & 3 (Figure 3 (b)) thanks to six-hole Kent chambers visible on Figure 3 (a). Holes are equally spaced along the azimuthal direction (every 60°). In addition, total pressure measurements are done with five-hole hemispheric probes at sections 2 & 4. Only 3 of the 5 holes are connected to pressure sensor to obtain ram pressure and right/left differential pressure. Druck pressure sensors and PT100 total temperature sensors are connected to a 34901A Multiplexer integrated in an Agilent 34970A

data acquisition system. Power factor, power and windmilling frequency are recorded by a VOLTECH PM3000A multi-meter which is also connected to the same multiplexer.
In turbine operation, an additional device is connected to the generating fan in order to apply different resistive loads, which enables to record several output power. This resistive bench is a purely resistive device (no inductance). The small pressure-ratio imposed by the windmilling fan makes difficult any accurate total temperature drop measurements. A total to static electromechanical efficiency is used for better estimation of the efficiency. General characteristics of the test bench (Table 2) give some details on its overall size.

length of the upstream assembly (2 fans + section adaptations)	2 000 mm	NFX test bench length (Section adaptations included)	3 000 mm
Carter length	600 mm		

Table 2. Test bench characteristics

III.4. Experimental approach

The fan characterization has been established by means of 10 speed lines. Each speed line has 8 dots which correspond to the 8 diaphragms used to change the operating point. The resulting set of data is a 10x8 array. For the fan experiment, 50 successive measurements (of the same operating point) on stabilized operating point have been recorded with an overall sampling frequency around 0.7 Hz. Arithmetic averaging is performed during the post process.
To run windmilling tests, the mass flow rate is controlled by two fans situated at the bench air intake (Figure 2 (b)). These fans are piloted simultaneously so that their rotational speeds are identical. A specific honeycomb treatment upstream of the windmilling fan inlet suppresses any gyration of the flow. Consequently, velocity profile is assumed to be uniform at the carter inlet.
The experimental programs of the two windmilling studies are identical. 8 piloting rotational speeds of the inlet fans have been tested as well as 10 resistive loads and 8 NFX diaphragms. Finally, experimental data are stored in a array of 8x10x8 dimension. For windmilling configurations, only 25 successive measurements (of the same operating point) have been done with the same sampling frequency (~ 0.7 Hz). Consequently, the acquisition time for one windmilling operating point is about 35 seconds. The stability of the fan operating point is such that dispersion of the successive measurements is found small. In addition, a sensitivity study of the sample size has been done and has demonstrated a statistic convergence of the data, even at this sample size.

III.5. Repeatability

Repeatability is studied on the average diaphragm for every rotational speed of the *Fan mode*. Most of the repeatability tests have been done on different days. Table 3 shows that the carried out experiments are repeatable with good accuracy.

	Confidence interval bounds ($I_{0.95}$)		*Interval size*
W^* (%)	99.58	100.28	0.70
Q^* (%)	78.76	79.90	1.14
η^* (%)	95.90	98.73	2.83
N^* (%)	78.98	79.11	0.12
$\pi_c{}^*$ (%)	99.91	100.23	0.32

Table 3. Confidence interval of the repeatability study

III.6. Numerical simulations

For the numerical investigations, the commercial FINE™/Turbo software developed by NUMECA is used. It solves the Reynolds-Averaged Navier-Stokes equations for the air considered as an incompressible perfect gas. Spatial discretisation is done with a Jameson centered second order scheme. A second order Runge-Kutta scheme was applied for time discretisation. Finally, resolution uses the SST model to achieve turbulence closure on a 1 million cell low Reynolds mesh ($y^+ \sim 1$) that models a single channel of the row. Rotor/stator interfaces are modeled as full non matching mixing planes.

Some details concerning the grid quality are presented Table 4. Most of the quality criteria are respected except skewness and angle of deviation. Minimum skewness of 15.6 deg is observed in the outlet bulb. However, the few involved cells are all concentrated on the same mesh line. Indeed, they come from the azimutal division of the full annulus in 23 passages: $Skew_{min} = \frac{360}{23} \approx 15.652$. As for the angle of deviation, maximum values are also reached very locally in the inlet bulb. The first inner cell width is set to 2 µm which leads to y^+ values around unity for the studied cases.

Grid quality criteria	Target value	Value	Location
Min skweness	>20 deg	15.652 deg	Outlet bulb (for $r \approx 0$)
Max aspect ratio	<2 000	1551	Row 2
Max expansion ratio	<2	1.957	Row 1
Max angle of deviation	<5	13.43 deg	Inlet bulb

Table 4. Grid quality

IV. Fan study results

The objective of this section is to give an overview of the fan characteristics by presenting compressor maps. Results of the fan experimental study are presented thanks to classical maps plotted in Figure 4.

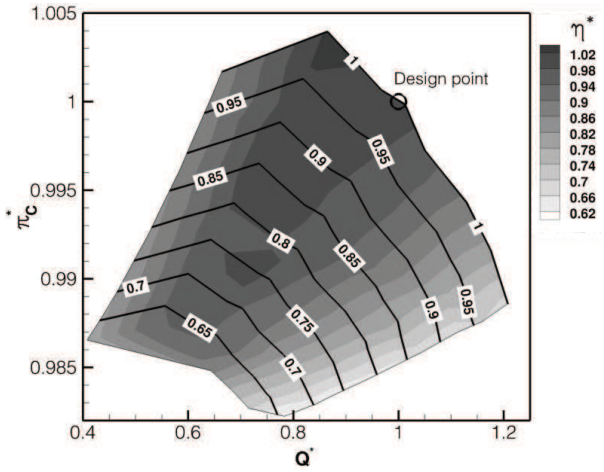

Figure 4. Compressor map

Results, as expected, are very classical and highlight the good functioning of the fan. Speed lines are plotted adimensioned by the nominal rotation speed. As indicated by the color map, color contours indicate normalized efficiency variations in the (Q^*, π_c^*) map. Figure 4 shows that the design point is almost located in the maximum efficiency regions and highlights the fan good design.

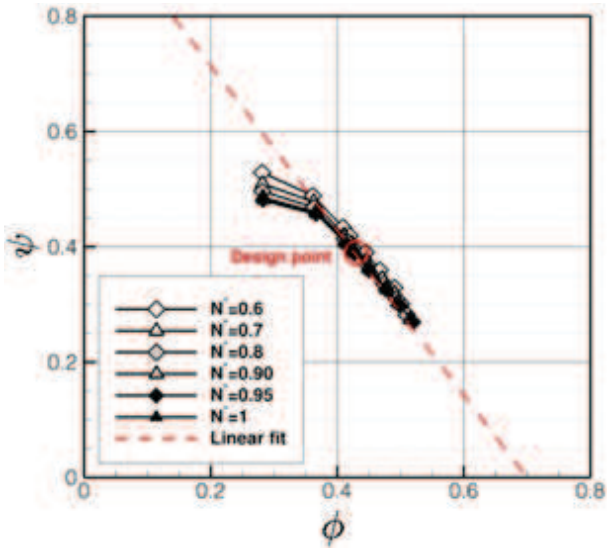

Figure 5. Fan characteristics in (ϕ, ψ)-chart

As stated before, the fan can be described according to eq. (8) in the (ϕ, ψ) chart. Figure 5 shows that its characterization is unique since every speed lines (N*) collapse on a single trend that is partially linear. Linear fit is added to experimental plots to highlight the linear tendency of experimental results and shows that there is a unique point (per speed line) out of the fit. This one is situated in the stall region in the (Q^*, π_c^*) map (Figure 4). The expected (linear) trajectory of the fan operation in the (ϕ, ψ) chart is thus observed. The influences of the rotational speed and of the compressibility are thus confirmed marginal. The ability of this geometry to recover some energy is now evaluated.

V. Windmilling study results

V.1. Direct Mode

Direct mode experimental results are presented in the (ϕ, ψ) map (Figure 6). The linear tendency observed for the *Fan Mode* is also visible for the *Direct mode*, and is in continuity with that of the *Fan Mode*. This was expected by the theoretical model, since Eq. (8) is valid for both of these modes, and depends only on the blade exit angle β_2, assuming that flow deviations are small. However, some deviations with the theoretical expectations are observed.

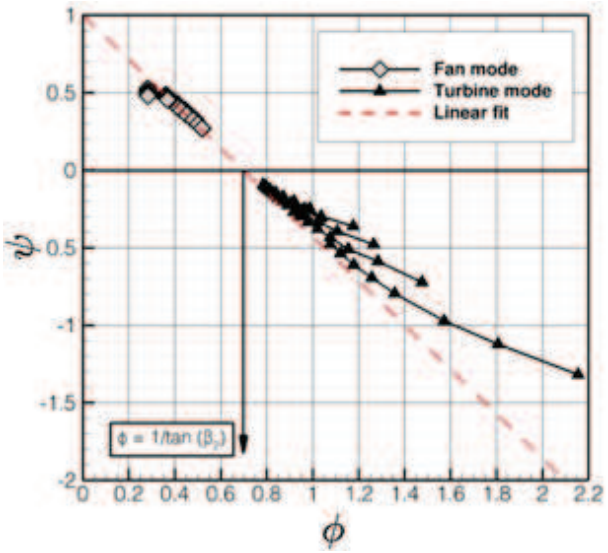

Figure 6. *Direct mode* (ϕ, ψ)-chart

Firstly, the linear behavior is lost for some operating points in windmilling. The most important deviations from the theoretical model correspond to the higher case of resistive load and to the higher rotational speeds. This can be partly explained by the hypothesis used to build the linear model. Indeed, the flow deviation, angle between the blade and the flow direction, is neglected. Yet, for a given rotational speed, increasing the axial velocity tends to amplify the flow separation at the pressure side of the rotor (and the suctions side of the stator). In fact, the *Direct mode* leads to poorly adapted flow at the rotor inlet so that a flow separation at the pressure side of this blade is observed on simulations (Figure 7). In addition, as reported in the literature, the flow in the stator is massively separated which tends to decrease the loading coefficient and to worsen the noticed discrepancy.
Secondly, the intercept of the linear evolution with the x-axis does not match the prediction based on the blades angles. This deviation is not fully understood, but the deviation of the flow at the trailing edge of the rotor making the geometrical angle non-representative of the flow angle is the most plausible origin.
Figure 6 also shows that it is impossible to recover fan-like power with the *Direct mode* since for a given ϕ the resulting loading coefficient is unique. In other word, negative loading coefficient cannot be reached for flow coefficient of the fan region (below ϕ=0.7). The strong separation of the diffuser observed on the Figure 7 is an additional penalty to the overall efficiency of the stage, which decreases furthermore the poor potential for energy recovery of this configuration.

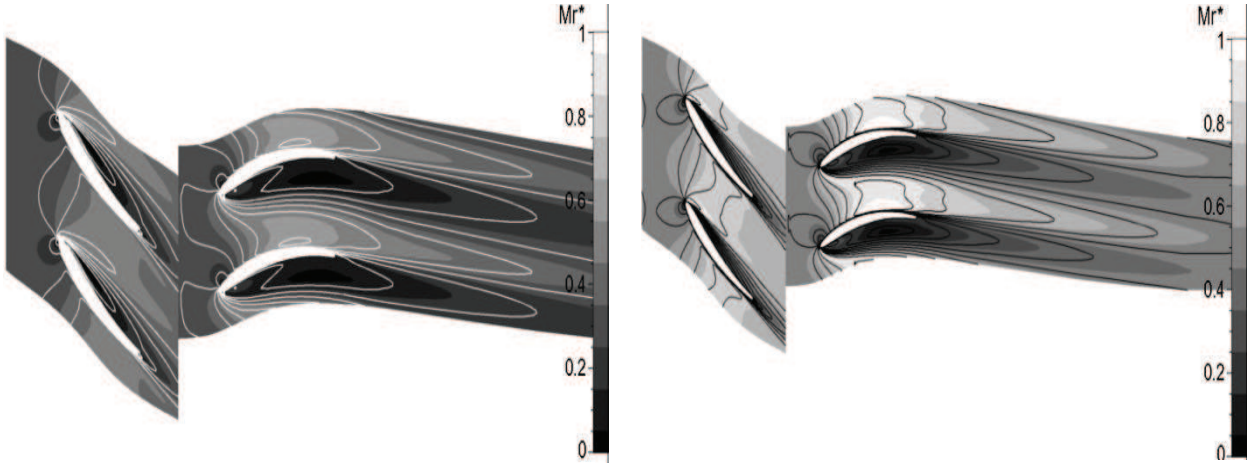

(a) **(b)**

Figure 7. Mid-span blade to blade relative Mach number (*Direct mode*), (a) Low efficiency operating point - (b) High efficiency operating point

V.2. Reverse Mode

Experimental (ϕ, ψ) characteristics of the *Reverse mode* are given in Figure 8. The first worth mentioning point concerns the difference between the two linear fits obtained. This comes from the fact that, in *Reverse mode*, the inlet swirl is not zero anymore, so that the reverse linear fit should follow the eq. (9) whereas fan and direct ones should follow eq. (8). Linear fits of experimental data are not completely following the linear model (not represented here) described by eq.(8) and eq.(9) for the reasons cited section V.1. Secondly, the main result of Figure 8 is that the flow coefficient of the fan and of the *Reverse mode* have a common interval of variation. This means that the *Reverse mode* is able to recover power in the fan domain of operation. Thirdly, the potential of power generation is related to the amplitude of the loading coefficient. It is clear that, for any given flow coefficient, the *Reverse mode* is far better than the direct one. For the highest values of the flow coefficient, the *Direct mode* potential seems to decrease while the reverse one seems to increase.

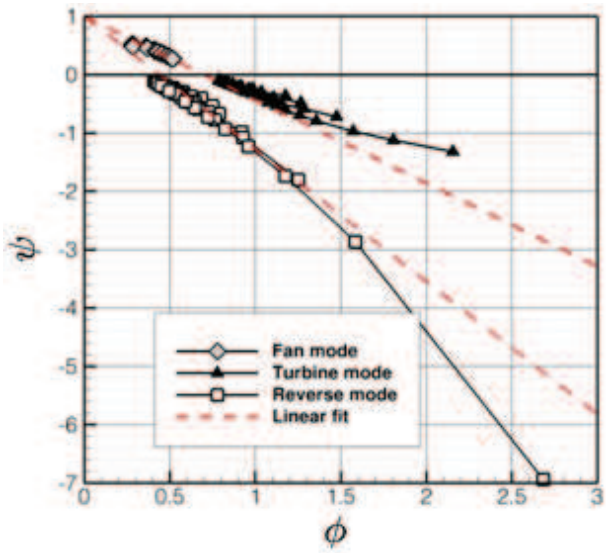

Figure 8. Global *(ϕ, ψ)* chart

The analysis of the numerical study explains the good performances of the *Reverse mode*. The reduced relative Mach number (Figure 9) in reverse configuration shows that the flow is always attached so that there is no vane blockage in this mode. Therefore, the reverse mass flow rate is likely to reach much higher *values* than the *Direct mode* one. For this reason, the rotational speed, and thus the output power, is expected to be higher in *Reverse mode*. This result is illustrated Figure 10.

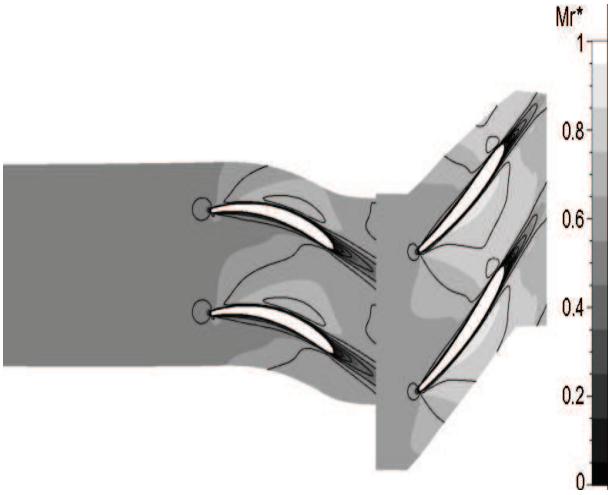

Figure 9. Reverse windmilling: relative Mach number (mid span)

As expected from the numerical analysis of the flow structures, the output power is higher for the reversed configuration than for the direct one. Figure 10, where the output power is given versus the mass flow rate, shows that the reverse configuration has an higher potential than the direct one. In this figure, small loading and high loading correspond to the applied resistive load. As mentioned above, for a given mass flow rate the *Direct mode* never enters the fan region whereas the *Reverse mode* does. The difference is quite important between the two configurations. The reversed mode is undeniably better in terms of output power than the *Direct mode*. The effects of the loading is also clearly marked. The higher the loading is, the higher the power increases.

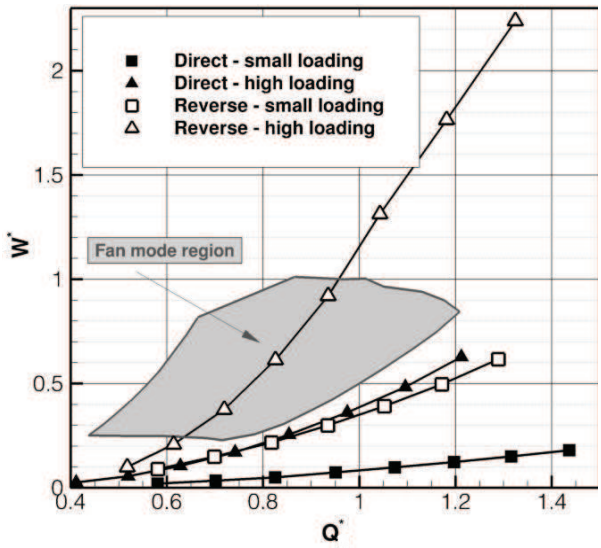

Figure 10. Power curves as a function of the mass-flow rate

VI. CONCLUSIONS

Fan tests show that the fan is working properly and that the design point is in the vicinity of the maximum efficiency region. Every experimental speed line of classical fan map collapsed in the (ϕ, ψ) representation. Experimental results can be fitted by linear tendency (called "linear fit"). The latter does not completely match with the theoretical linear model for three main reasons. First, flow angles at the rotor exit are different of blade angles and flow deviation cannot be neglected. Second, axial velocity is supposed constant through the rotor which is not totally accurate. Taking into account the acceleration parameter could decrease the differences observed between the fit and the model. Third, the incompressibility hypothesis assumed from the beginning is questionable.

As for the windmilling modes, they are compared on the output power basis and on their potential of power generation. This potential is evaluated in terms of the maximum value of the output power for a given operating point. Some theoretical developments show that the expression of the fan operations should be expressed in a (ϕ, ψ) map. In such representations, potential of power generation is evaluated on the loading coefficient amplitude. In both representations, experimental results show that the potential of the *Reverse mode* is the far higher than the *Direct mode* one. Numerical results have qualitatively explained the difference between the two modes through the presentation of flow patterns.

REFERENCES

1 ESDU series (1981), Data Item 81009, ISBN 978 0 85679 334 9, Estimation of windmilling drag and airflow of turbo-jet and turbo-fan engines, Amendment A, pp1-20

2, Zhao. Qi. Shou, CALCULATION OF WINDMILLING CHARACTERISTICS OF TURBOJET ENGINES, *Journal of Engineering for Power*, January 1981, **103**, pp. 1-12

3 W. Braig, H. Schulte, and C. Riegler, COMPARATIVE ANALYSIS OF THE WINDMILLING PERFORMANCES OF TURBOJET AND TURBOFAN ENGINES, *Journal of propulsion and power*, March-April 1999, **15**, No. 2,

4 Dilip Prasad, and Wesley K. Lord, INTERNAL LOSSES AND FLOW BEHAVIOR OF A TURBOFAN STAGE AT WINDMILL, *Journal of Turbomachinery*, 2010, **132**, pp. 031007-1/031007-10

5 A. Gill, T. W. von Backström, and T. M. Harms, Reverse flow turbine like operation of an axial flow compressor, *Proceedings of ASME Turbo Expo 2012*, GT2012-68783

6 Lakshminarayana B., 1996, *Fluid dynamics and heat transfer of turbomachinery*, John Wiley. & Sons,

7 Norme ISO 5801, Décembre 1999, *Ventilateurs industriels -- Essais aérauliques sur circuits normalisés*